

# Single-cell transcriptomic analyses reveal cellular and molecular patterns of rubber tree response to early powdery mildew infection

Xiaoyu Liang<sup>1</sup>  | Zhan Ma<sup>1</sup> | Yuhang Ke<sup>1</sup> | Jiali Wang<sup>1</sup> | Lifeng Wang<sup>2</sup> | Bi Qin<sup>2</sup> | Chaorong Tang<sup>1</sup> | Mingyang Liu<sup>1</sup> | Xuemei Xian<sup>1</sup> | Ye Yang<sup>1</sup> | Meng Wang<sup>1</sup> | Yu Zhang<sup>1</sup>

<sup>1</sup>College of Tropical Crops, Sanya Nanfan Research Institute, College of Plant Protection, Hainan University, Haikou, China

<sup>2</sup>Rubber Research Institute, Chinese Academy of Tropical Agricultural Sciences, Haikou, China

## Correspondence

Yu Zhang and Meng Wang, College of Tropical Crops, Sanya Nanfan Research Institute, College of Plant Protection, Hainan University, Haikou, China.

Email: [yuzhang\\_rain@163.com](mailto:yuzhang_rain@163.com) and [wangmeng@hainanu.edu.cn](mailto:wangmeng@hainanu.edu.cn)

## Funding information

Modern Agro-industry Technology Research System (CARS-33-BC1); National Natural Science Foundation of China (32160370; 32160654); Natural Science Foundation of Innovative Research Team Project of Hainan province (322CXTD506)

## Abstract

As a perennial woody plant, the rubber tree (*Hevea brasiliensis*) must adapt to various environmental challenges through gene expression in multiple cell types. It is still unclear how genes in this species are expressed at the cellular level and the precise mechanisms by which cells respond transcriptionally to environmental stimuli, especially in the case of pathogen infection. Here, we characterized the transcriptomes in *Hevea* leaves during early powdery mildew infection using single-cell RNA sequencing. We identified 10 cell types and constructed the first single-cell atlas of *Hevea* leaves. Distinct gene expression patterns of the cell clusters were observed under powdery mildew infection, which was especially significant in the epidermal cells. Most of the genes involved in host-pathogen interactions in epidermal cells exhibited a pattern of dramatically increased expression with increasing pseudotime. Interestingly, we found that the *HbCNL2* gene, encoding a nucleotide-binding leucine-rich repeat protein, positively modulated the defence of rubber leaves against powdery mildew. Overexpression of the *HbCNL2* gene triggered a typical cell death phenotype in tobacco leaves and a higher level of reactive oxygen species in the protoplasts of *Hevea* leaves. The *HbCNL2* protein was located in the cytomembrane and nucleus, and its leucine-rich repeat domain interacted with the histidine kinase-like ATPase domain of the molecular chaperone *HbHSP90* in the nucleus. Collectively, our results provide the first observation of the cellular and molecular responses of *Hevea* leaves to biotrophic pathogen infection and can guide the identification of disease-resistance genes in this important tree species.

## KEY WORDS

*HbCNL2*, *Hevea brasiliensis*, infection response, protein interaction, single-cell atlas

Xiaoyu Liang, Zhan Ma, and Yuhang Ke contributed equally to this study.

## 1 | INTRODUCTION

Rubber tree (*Hevea brasiliensis* Muell. Arg.) has historically been the only economically accessible source of natural rubber. As a perennial woody plant, rubber trees must respond to numerous biotic and abiotic stresses, including pathogens, drought, cold, and wind. Due to the limited utilization of germplasm during the early periods of rubber tree breeding, almost all commercial rubber cultivars are clones containing a narrow genetic base (Priyadarshan & Goncalves, 2003). Thus, commercial rubber cultivars are susceptible to pathogens, among which powdery mildew is a major threat (Wan et al., 2014). Powdery mildew affects rubber-growing areas worldwide, resulting in the premature fall of young leaves. The disease caused by *Oidium heveae* is severe in regions with a subtropical climate including China and results in rubber yield losses of up to 45% (Liyanage et al., 2016). The utilization of resistance genes in crop breeding programs could efficiently and economically control the occurrence of powdery mildew (Li et al., 2020). Due to the lack of knowledge of the molecular mechanisms and key genes of resistance to rubber tree disease, all rubber-growing countries still use crossbreeding methods to develop disease-resistant clones (Narayanan & Mydin, 2012). These long-term breeding methods and the undefined resistance pathway cause great difficulties in the development of superior cultivars. Therefore, there is a need to clarify the molecular regulatory network of rubber trees in response to *O. heveae* infection, to screen and identify relevant pathogen resistance genes, and to develop molecular breeding methods for disease resistance.

The nucleotide-binding leucine-rich repeat (NLR) genes, which encode proteins with nucleotide-binding sites and leucine-rich repeat (LRR) domains, account for the majority of plant disease resistance genes that have been cloned to date. These proteins are classified into two primary subfamilies: toll-interleukin-like receptor domain-containing (TNL) and coiled-coil domain-containing (CNL) (van Wersch et al., 2020). CNL proteins perform important roles in the innate immunological defence of plants against powdery mildew. Many of the mildew locus A (MLA) genes and powdery mildew resistance (*Pm*) genes that encode CNL proteins have been cloned and identified in monocotyledonous crops wheat and barley (Seeholzer et al., 2010; Li et al., 2020). The *Arabidopsis* broad-spectrum mildew resistance gene *RPW8*, which encodes a CNL protein, enhances powdery mildew resistance in the dicotyledon crop grapevine (Hu et al., 2018; Xiao et al., 2001). However, there is a gap in research related to *Hevea* CNL proteins against powdery mildew, which needs to be screened and validated.

Single-cell RNA sequencing (scRNA-Seq) has just started to be applied in diverse aspects of plant science. Its high-resolution molecular information contributes to elucidating the biological function of genes and the molecular mechanisms controlling their expression (Rich-Griffin et al., 2020). With this technology, it is possible to explore the heterogeneity among different cell types in complex tissues and to identify unknown cell types. Many single-cell transcriptomic atlases have been established successfully for various

crops, including rice, maize, peanuts and tea (Liu et al., 2021; Wang et al., 2021; Wang et al., 2022; Xu et al., 2021). These atlases lay the foundation for the functional characterization and manipulation of candidate genes that are needed to develop elite cultivars. In addition to revealing the gene expression atlas, single-cell transcriptomics is also used to investigate plant responses to biotic and abiotic stress (Bai et al., 2022; Jean-Baptiste et al., 2019). The advancement of cell type-specific transcriptomics reveals crucial plant cellular processes involved in stress adaptation (Dinneny et al., 2008). This technology has provided a previously unattainable view of gene expression dynamics in plant tissues and the alteration of these dynamics under various physiological conditions (Rich-Griffin et al., 2020). Single-cell transcriptomic analysis of plant tissues exposed to pathogen invasion will be helpful in identifying major cell clusters involved in immune resistance pathways (Liu et al., 2021).

Here, we constructed the first single-cell transcriptomic atlas for the rubber tree and identified cluster-specific marker genes for each type of rubber leaf cell. Based on the expression patterns for cell lineage responses to *O. heveae* infection, we characterized pathways and genes associated with disease resistance. Notably, the NLR gene *HbCNL2* was identified as positively correlated with *Hevea* leaf defence against *O. heveae* for the first time, revealing that the classic defence response model is also conserved in rubber trees. In brief, we have provided an example of the application of single-cell transcriptomics analysis in studying the complex regulation of plant disease resistance in rubber trees.

## 2 | MATERIALS AND METHODS

### 2.1 | Plants and fungal treatment

The experiment was performed using seedlings of the rubber tree variety Reyan73397, a commonly cultivated genotype in China. One-year-old rubber seedlings, approximately 50 cm tall with 20 branches, were obtained from the experimental plantation of the Chinese Academy of Tropical Agricultural Sciences (Danzhou, Hainan, China) and cultivated in 10-L pots (one plant per pot) filled with turf soil in a greenhouse. The powdery mildew pathogen *O. heveae* strain HO-1 was single-spore isolated and purified from the rubber nursery and maintained on the Reyan73397 seedlings. For inoculation, fresh conidial spores were dusted from the surface of infected leaves and collected into a sterile centrifuge tube (Liang et al., 2018). Conidia were washed in sterile water, counted with a hemocytometer, and diluted to  $10^5$  spores mL<sup>-1</sup>. One branch of each rubber seedling was sprayed with the conidial suspensions and 0.5% Tween 80, while another branch of the same seedling was sprayed with ddH<sub>2</sub>O and 0.5% Tween 80 as a control. The rubber seedlings were then grown at 22–24°C with approximately 80% humidity and a 14-h light/10-h dark cycle. The three bronze leaves on the treated branches were harvested at 8- and 36-hours post inoculation (hpi) for immediate protoplast isolation.

## 2.2 | Rubber leaf protoplast isolation and single-cell complementary DNA (cDNA) library construction

The extraction of rubber leaf protoplasts was performed according to the standard method reported by Zhang et al. (2016). Using a hemocytometer, the density of the protoplasts was calculated and set to  $700\text{--}1500 \text{ cells } \mu\text{L}^{-1}$ . Fluorescein diacetate and trypan blue staining were used to measure the activity of single-cell suspensions, and protoplasts with activity levels greater than 80% were chosen for further investigation. The protoplasts of four samples were processed and analyzed by a 10 $\times$  Genomics GemCode Single-cell instrument, generating single-cell Gel Bead-In-EMulsion (GEMs). Libraries were generated and sequenced from the cDNAs with Chromium Next GEM Single Cell 3' Reagent Kits v3.1. The libraries were then pooled and sequenced on an Illumina NovaSeq. 6000 by Genedenovo Biotechnology Co., Ltd. The raw data were converted to FASTQ files and underwent alignment and count quantification with 10X Genomics Cell Ranger software (10x Genomics, version 3.1.0). Single-cell FASTQ sequencing reads were mapped to the *Hevea* Reyan73397 genome (ASM165405v1).

## 2.3 | Data visualization and clustering

The raw count matrices were imported into Seurat version 3.1.1 for downstream analysis. Before analyzing the data, we filtered out cells with an unusually high number of unique molecular identifiers ( $\text{UMIs} \geq 8000$ ) or mitochondrial gene percent ( $\geq 10\%$ ). We used a method called 'LogNormalize' for global-scaling normalization, which multiplies the measurements of each cell's gene expression by the total expression, multiplies this by a scale factor (10 000 by default), and log-transforms the data. For dimensionality reduction, principal component analysis was employed. T-distributed stochastic neighbor embedding and uniform manifold approximation projection were generated to visualize clusters (Becht et al., 2019; Maaten & Hinton, 2008). The log-normalized matrices were then loaded onto SingleR R packages for cell type annotation, which is based on correlating gene expression of reference cell types with single-cell expression.

## 2.4 | Differentially expressed genes (DEGs) and functional enrichment analysis

The FindMarkers function in Seurat was used to DEGs between samples based on a dual threshold of  $|\log_{2}\text{FC}| \geq 0.8$ . The intersections of DEGs between samples were visualized using the UpSetR function (Conway et al., 2017). DEGs in each sample were annotated using the biological process of gene ontology (GO) terms based on the reference genome. GO analyses and Kyoto Encyclopedia of Genes and Genomes (KEGG) pathway analyses were performed using the clusterProfiler package (version: 3.18.0) (Yu et al., 2012).

## 2.5 | Pseudotime trajectory analysis

The expression matrix of epidermal subcluster cells was used to run a separate pseudotime analysis with Monocle version 2.0. We identified key genes related to the development and differentiation processes with a false discovery rate  $< 0.05$  and grouped genes with similar trends in expression. We also performed KEGG/GO enrichment analysis to uncover the regulatory network and functional genes.

## 2.6 | Real-time reverse transcription PCR (qRT-PCR) analysis

For qRT-PCR validation of cell types, three replicates of epidermal, mesophyll, vascular and latex tissues were isolated from rubber leaves, respectively. The epidermal layers were collected using tweezers. The leaves without epidermis were dissected to separate the vasculature (mainly including xylem and phloem), while exuded latex was collected. Mesophyll tissue was collected from the remaining leaves. For qRT-PCR analysis of CNL genes, leaves of the 18 *Hevea* varieties selected for this study were collected from the experimental plantation of the Rubber Research Institute of the Chinese Academy of Tropical Agricultural Sciences. All leaf tissues were frozen in liquid nitrogen and stored at  $-80^{\circ}\text{C}$  for total messenger RNA extraction and reverse transcription. Total RNA was extracted using the Polysaccharide Polyphenol Plant Total RNA Extraction Kit (TIANGEN). Reverse transcription PCR was performed with HiScript II qRT SuperMix for qPCR (Vazyme). qRT-PCR was performed using ChamQ Universal SYBR qPCR Master Mix (Vazyme) on a Bio-Rad CFX Connect instrument. The qRT-PCR primers are listed in Supporting Information: Table S1. Gene expression was normalized using two housekeeping genes *HbActin* and *Hb18S*.

## 2.7 | Phylogenetic analysis

The amino acid sequences of CNL proteins of wheat, barley, and *Dasypyrum* for powdery mildew resistance were queried in the NCBI protein database, and a BLASTP search was performed on the rubber tree genome sequence. The final data set of *Hevea* NLR proteins was obtained by removing redundant and incomplete sequences. Amino acid sequence alignment was performed with ClustalW software and MEGA version 10.0.5 with the default parameters. The maximum likelihood method (1000 bootstrap tests) was then used to create a phylogenetic tree based on the alignment data.

## 2.8 | Subcellular localization

Subcellular localization of the HbCNL2 protein was performed according to a previously published method (Liu et al., 2022). Briefly, the coding sequence of HbCNL2 was cloned into the pGREEN vector

(with the 35S × 2Pro strong promoter and green fluorescent protein [GFP] tag). The primers for vector construction are listed in Supporting Information: Table S1. Using the electroshock approach, the *Agrobacterium* strain GV3101 was transformed with a recombinant vector and an empty vector. One day in advance, 5-week-old tobacco (*Nicotiana benthamiana*) was cultured under consistent growth conditions and water in the dark and was then injected with *Agrobacterium*. GFP signal was detected after excitation at 488 nm with a 500–550-nm emission filter. The leaves were stained with 4,6-diamino-2-phenylindole (DAPI), and its signal was detected after excitation at 405 nm with a 445–450-nm emission filter. Lactophenol-trypan blue staining was used to assess the viability of the tobacco cells after HbCNL2 injection (Keogh et al., 1980). The percentage of the stained area was measured using ImageJ. The statistical results were generated using three independent biological preparations.

## 2.9 | Intracellular reactive oxygen species (ROS) analysis

The coding sequence of HbCNL2 was cloned into the mScarlet vector (with the 35S × 2Pro strong promoter). The primers for vector construction are listed in Supporting Information: Table S1. Ten micrograms of recombinant vector were added to 200 µL protoplasts of *Hevea* leaves for transformation, which was conducted using the PEG4000-mediated transformation method (Zhang et al., 2016). Intracellular ROS analysis was performed using an oxidant-sensitive probe, 2',7'-dichlorofluorescein diacetate (DCFH-DA) (Biyuntian). The protoplasts were incubated with DCFH-DA in a water bath at 37°C for 25 min. ROS levels were detected with a fluorescence microplate reader and expressed as relative fluorescence unit.

## 2.10 | Protein interaction assays

Luciferase complementation assay (LCA) and bimolecular fluorescence complementation (BiFC) assays between HbCNL2, the heat shock protein 90 (HbHSP90) and the suppressor of the G2 allele of SKP1 (HbSGT1b) were performed according to a previously published method (Liu et al., 2022). The primers for vector construction are listed in Supporting Information: Table S1. For LCA, the coding sequence of HbCNL2 was inserted into the pCAMBIA1300-nLUC vector, while the coding sequences of HbHSP90 and HbSGT1b were inserted into the pCAMBIA1300-cLUC vector. These constructed vectors were transformed into *Agrobacterium* strain GV3101 and injected into tobacco. After exposure to light following 12 h of darkness, plants were grown and monitored for 48 h. During observation, d-luciferin potassium salt was injected into each region on the dorsal side of the leaf. Leaf luminescence was measured in a live plant molecular imaging system (Princeton Instruments). For the BiFC assay, HbCNL2 and HbHSP90 coding sequences were introduced into 35S::SPYCE nYFP and

35S::SPYNE cYFP vectors, respectively. The *Agrobacterium* treatment and tobacco culture were performed as described above. YFP signal was detected after excitation at 510 nm with a 520–570-nm emission filter. Three biological replicates of tobacco were selected for fluorescence detection.

## 2.11 | Statistical analysis

IBM-SPSS 26.0 statistical software was used for the statistical analysis. Duncan's multiple range test was applied to compare the significant differences among the expression levels, and Tukey's honestly significant difference test was used to compare the significant differences between all treatments against their controls.

## 3 | RESULTS

### 3.1 | Protoplast isolation and scRNA-Seq

To construct the single-cell atlas for the rubber tree, we isolated protoplasts from *Hevea* leaves and performed scRNA-Seq (Figure 1a). The rubber leaves were harvested at 8 and 36 hours postinoculation (hpi) with or without *O. heveae* inoculation, and the samples were named T8 (8 hpi with pathogen inoculation), T36 (36 hpi with pathogen inoculation), C8 (8 hpi without pathogen inoculation) and C36 (36 hpi without pathogen inoculation). The protoplast concentration of all samples exceeded 1000 cells µL<sup>-1</sup>, and the proportion of viable cells exceeded 85%, indicating that these protoplasts were suitable for the preparation of single-cell transcription profiles (Supporting Information: Figure S1). The isolated cells were subsequently analyzed with the 10x Genomics Chromium platform. We isolated a single-cell transcriptome of 44 102 cells from these four samples after deleting duplicate cells and cells of low quality. The transcriptome contains more than 400 million reads in each sample, over 85% of which are mapped to the *Hevea* Reyan73397 genome (ASM165405v1). The average median number of UMIs per cell was 8606, and the average median number of genes per cell was 3756. An overview of quality control parameters for single-cell transcriptomes is provided in a statistical table (Supporting Information: Table S2).

### 3.2 | Leaf cell atlas generation

We performed unsupervised cluster analysis on total cells from four samples and identified 18 clusters with high cellular heterogeneity (Figure 1b). The number of cells distributed in each cluster ranged from 700 to 6020 (Supporting Information: Table S3). Currently, genetic databases lack multiple cell-specific markers with specific biological functions and expression patterns for rubber trees. To faithfully annotate 18 cell clusters, we searched for homologous genes in rubber trees using known single-cell markers (Supporting

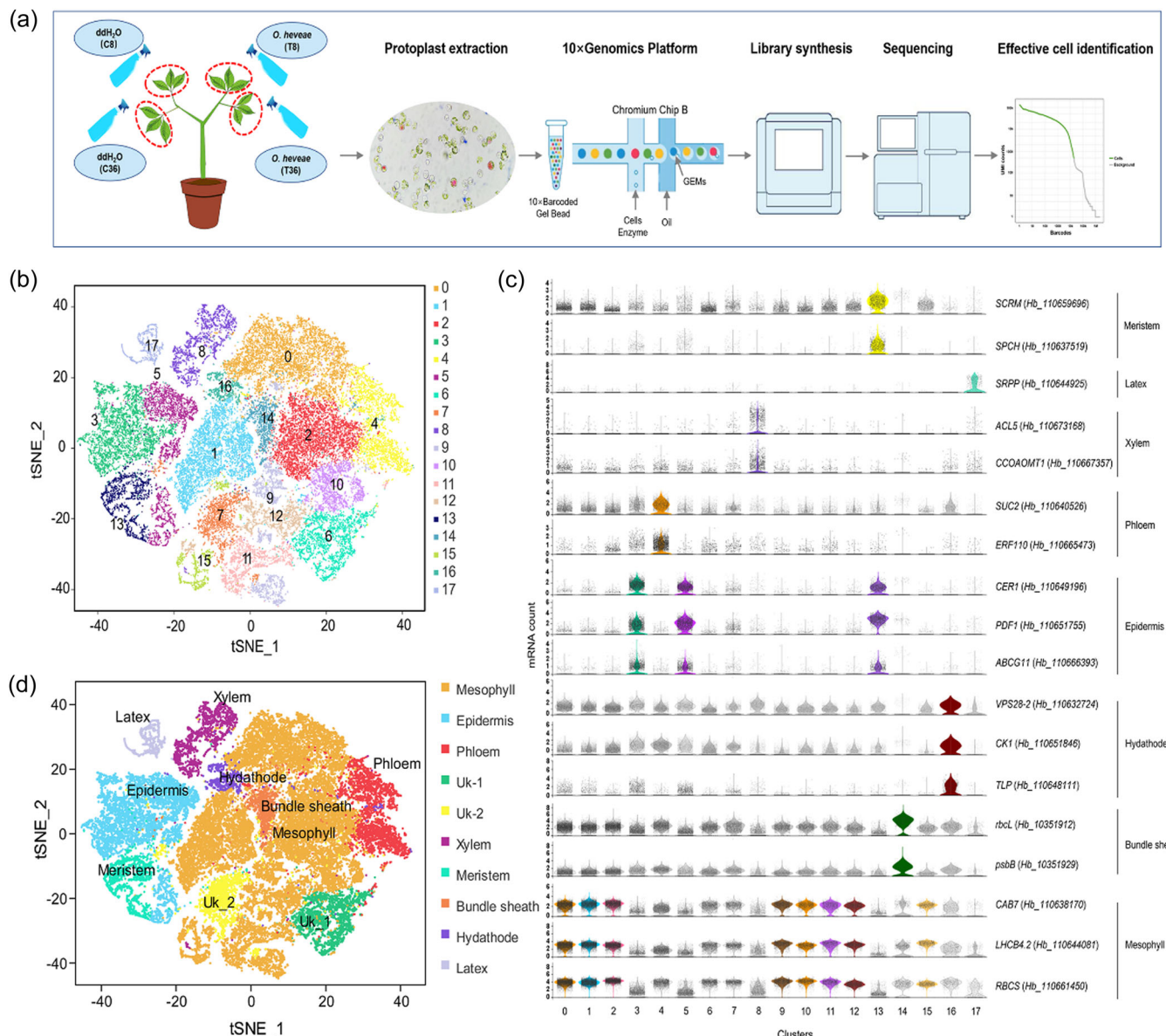


**FIGURE 1** Isolation and cluster analysis of single-cell transcriptomes from rubber tree leaves. (a) Protocol of single-cell library preparation. Protoplasts were obtained by enzymatic hydrolysis. GEMs were created by combining mRNA released when a single-cell solution burst with a gel bead and an emulsion. Each GEM reverse-transcribed the cell's mRNA, and then the tagged cDNA was combined and amplified to create the library. (b) tSNE visualization of the 18 cell clusters identified by unsupervised clustering analysis. (c) Violin diagram of the expression distribution of marker genes. (d) Visualization of the 10 cell clusters using tSNE based on marker gene analysis. cDNA, complementary DNA; GEM, gel bead-in-emulsion; mRNA, messenger RNA; tSNE, t-distributed stochastic neighbor embedding.

Information: Table S4). The transcription factors SCRM and SPCH are two known meristem-related genes involved in the division and differentiation of leaf primordia cells (Liu et al., 2020; de Marcos et al., 2017). Small rubber particle protein (SRPP) is known to be involved in the regulation of natural rubber biosynthesis (Feng et al., 2016). The ACL5 gene encoding thermospermine synthase is expressed explicitly in xylem vessel cells, and the CCOAOMT1 gene is involved in lignin production (Kim et al., 2021; Li et al., 2021). The ethylene-responsive factor ERF110 is involved in phloem formation, and the phloem-specific sucrose transporter SUC2 was identified as a phloem marker gene (Gottwald et al., 2000; van Raemdonck et al.,

2005). CER1 is specifically expressed in the epidermis of aerial organs and was used as a marker gene of epidermal tissue along with PDF1 and ABCG11 (Bourdenx et al., 2011; Satterlee et al., 2020). Vacuolar sorting-associated protein VPS28-2, choline kinase CK1 and thaumatin-like protein TLP are highly specific for hydathode cells (Kim et al., 2021; Satterlee et al., 2020). Bundle sheath cells encircled the xylem and phloem cell populations, consistent with the expression levels of the *rbcL* and *psbB* genes (Satterlee et al., 2020; Stoppel et al., 2011). Photosynthesis in mesophyll cells is primarily mediated by ribulose bisphosphate carboxylase small chain, chlorophyll a-b binding protein CAB7 and light-harvesting chlorophyll a-b

binding protein LHC4.2 (Tsutsumi et al., 2006). Based on the expression patterns of these marker genes shown in Figure 1c and Supporting Information: Figure S2, we identified 10 cell types: meristem cells (cluster 13), latex cells (cluster 17), xylem cells (cluster 8), phloem cells (cluster 4), hydathode cells (cluster 16), bundle sheath cells (cluster 14), epidermis cells (clusters 3 and 5) and mesophyll cells (clusters 0, 1, 2, 9, 10, 11 and 12). The cell types of clusters 6 and 7 could not be determined using the current marker genes and were named unknown cells (Figure 1d). The rubber leaf cell atlas contributes to the further characterization of the fundamentals of these specific cell types and the analysis of cellular heterogeneity.

### 3.3 | Cell cluster identification

GO analysis was used to verify the biological processes of these 10 cell clusters (Figure 2a). We found that different biological processes were significantly enriched in distinct cell types ( $p < 0.05$ ). For example, mesophyll cells were enriched for photosynthesis-related biological processes. Lignin metabolism, cuticle development and fatty acid biosynthesis were all enhanced in the epidermis. The vascular system, including the bundle sheath, phloem and xylem, was enriched in signal transduction and ion transport processes. Therefore, visualization of cell expression allowed for more intuitive validation of cell types. The classification of rubber leaf cells was further verified by qRT-PCR experiments (Figure 2b). Easily isolated tissues of rubber leaves, such as epidermis, mesophyll, vascular and latex, were obtained for qRT-PCR tests. We proved that CER1, PDF1 and ABCG11 were highly expressed in the epidermis, that SRPP was highly expressed in latex, that CAB7 and LHC4.2 were highly expressed in mesophyll cells and that ACL5 and SUC2 were highly expressed in vascular cells. The

expression patterns of marker genes showed the best agreement with the violin diagram results.

After successfully identifying cell subsets, we collected the top five most highly expressed genes in each of the 10 clusters. These 50 genes showed cluster-specific expression in the heatmap (Supporting Information: Figure S3). For example, the epidermis-specific gene LOC110673595 encodes a GDSL esterase/lipase, which is highly abundant in the epidermis during leaf elongation (Girard et al., 2012; Reina et al., 2007; Yeats et al., 2010). The phloem-specific gene STP13 encodes a sugar transport protein that contributes to long-distance sugar transportation in plants (Lu et al., 2018; Zhao et al., 2004). The xylem-specific gene WAT1 encodes a plant-specific protein that regulates the secondary cell wall thickness of wood fibres (Palit et al., 2020). These three genes show tissue-specific expression consistent with their biological functions (Supporting Information: Figure S4). Finally, we constructed a cluster-specific marker gene library of rubber tree leaves (Supporting Information: Table S5). The novel genes we identified will contribute to further studies on the molecular biology of rubber tree cells.

### 3.4 | Single-cell heterogeneity analysis of rubber leaves infected by *O. heveae*

Revealing cell-to-cell heterogeneity is critical for studying plant responses to biotic stress. We first characterized the single-cell expression profiles of rubber leaves infected by *O. heveae*. The interaction of the expression profiles was explored by comparing how various cell types respond to infection (Supporting Information: Figure S5). The analysis of cell proportions between the two subgroups of the control (C) and treatment (T) showed that the rubber leaves responded markedly to the *O. heveae* stimulus

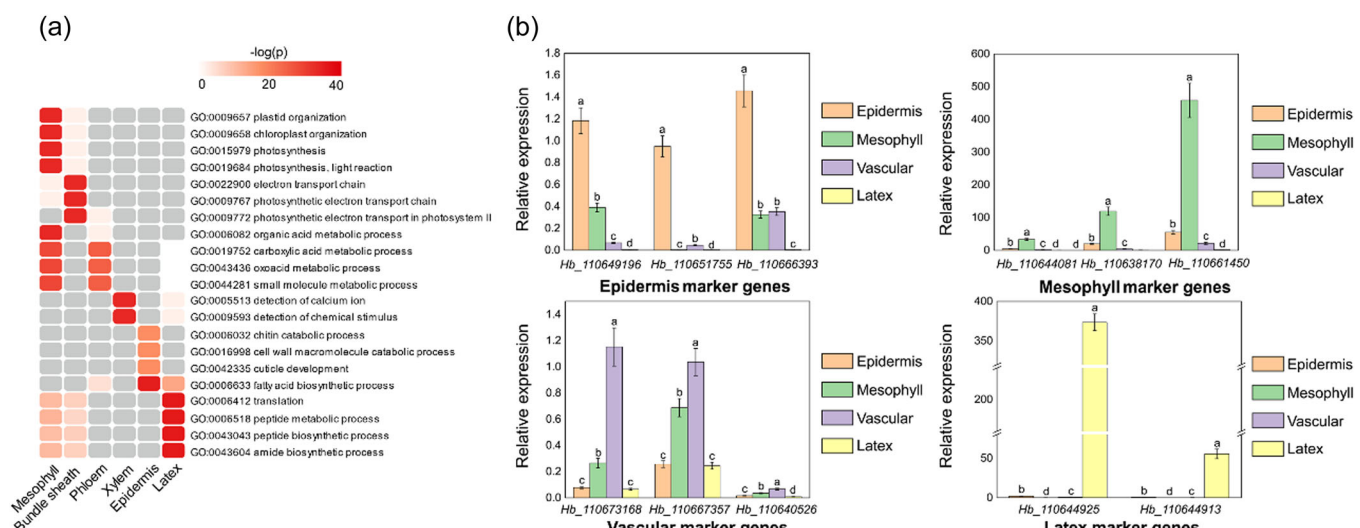


**FIGURE 2** Cell cluster identification of single-cell transcriptomes from rubber tree leaves. (a) Tissue-specific GO terms in different cell types ( $p \leq 0.05$ ). (b) Expression of epidermal, mesophyll, vascular and latex tissue-specific marker genes. Columns with different lowercase letters denote significant differences at the  $p < 0.05$  level. GO, gene ontology. [Color figure can be viewed at [wileyonlinelibrary.com](http://wileyonlinelibrary.com)]

(Supporting Information: Table S6). In particular, epidermal cells and meristem cells displayed comparable expression patterns and differed significantly from other cell types (Figure 3a). There was a significant increase in the proportion of epidermal cells, while the proportion of mesophyll cells was reduced (Figure 3b). The UMI analysis indicated that different cell clusters exhibited distinct transcriptional characteristics during *O. heveae* infection (Figure 3c; Supporting Information: Table S7). To determine the level of transcriptional heterogeneity, we identified the regulation of DEGs in specific cell types at 8 (T8 compared to C8) and 36 hpi (T36 compared to C36) (Supporting Information: Tables S8 and S9). Meristem cells and hydathode cells have greater DEG percentages than the other six known cell types (Figure 3d). There was some overlap of DEGs across different cell types, but the DEGs mainly appeared in a single cell type (Figure 3e).

### 3.5 | Characterization of expression profiles for cell lineage responses to *O. heveae* infection

To gain insight into the expression patterns of cell genes responding to *O. heveae* stimulus, we further performed GO and KEGG pathway analysis on these DEGs at different time points of infection in specific cell types. At 8 hpi, 20 of the immune-related GO terms were significantly enriched and down-regulated in 10 cell subsets. Hydathode, epidermis and meristem subgroups were the most enriched in GO terms, including those involved in detoxification, response to toxic substances, oxidation-reduction processes and

hydrogen peroxide metabolic processes (Figure 4a). At 36 hpi, most immune-related GO terms were significantly upregulated and were mainly enriched in the hydathode and epidermis subgroups (Figure 4b). Interestingly, there were eight repeats in these immune-related GO terms at 8 and 36 hpi. In other words, these biological processes were inhibited by *O. heveae* infection at the early stage (8 hpi) but were upregulated at a later stage (36 hpi). In KEGG analysis, DGEs involved in photosynthesis, photosynthesis-antenna proteins, carbon metabolism and carbon fixation in photosynthetic pathways were significantly down-regulated in various cell subsets at 8 hpi, but these terms were not enriched at 36 hpi (Table 1).

### 3.6 | Pseudotime trajectory analysis of epidermal cells during the different stages of *O. heveae* infection

Powdery mildews mainly invade the epidermal cell layer of leaf tissues, in which they form haustorial structures and deliver effectors to the invaded cells to suppress plant immune responses (Lambertucci et al., 2019). To assess the expression profiles of rubber leaves at the early and late stages of infection, we performed a pseudotemporal analysis of epidermal cells after *O. heveae* infection. The gene expression matrices of epidermal cells generated from samples T8 and T36 were used to construct the differentiation trajectory (Figure 5a). The results showed that the pseudotime trajectory has three branch points that divide all cells into seven states. The cells shifted gradually from state 1 to state 4 as the

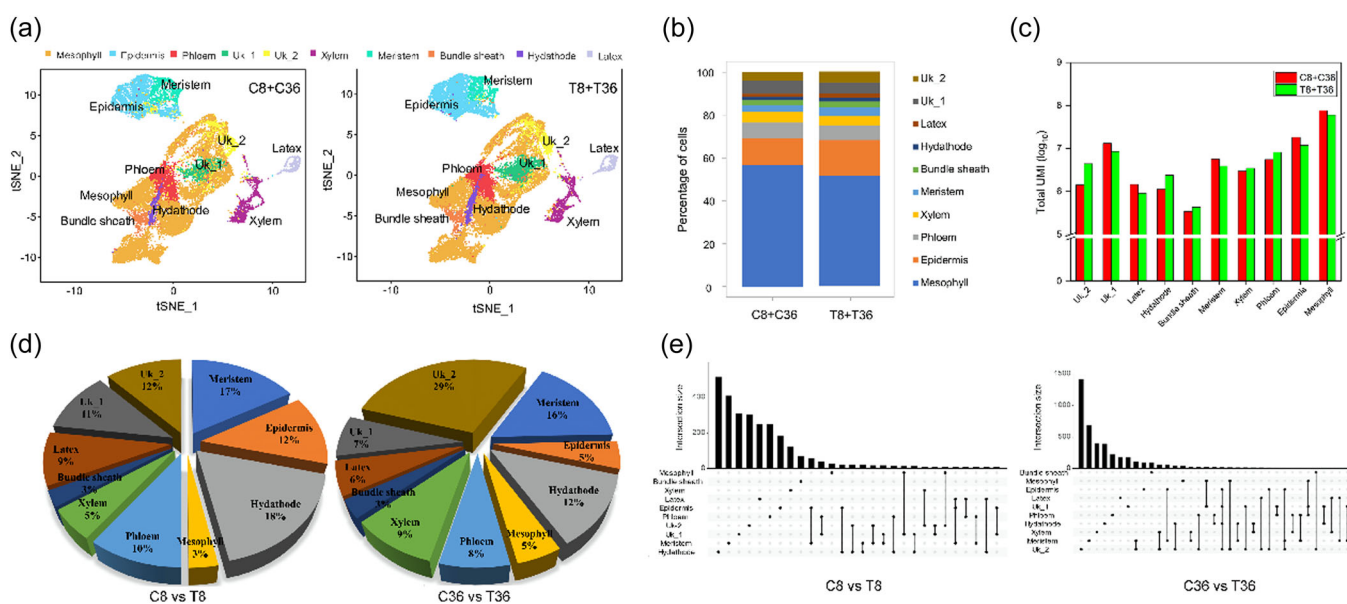


**FIGURE 3** Single-cell transcriptome analysis of control and infected samples. (a) UMAP plot of separated single cells of the C8 + C36 samples and the T8 + T36 samples. (b) The relative proportion of each cell type in the C8 + C36 samples and the T8 + T36 samples. (c) UMI values of each cell type. (d) The proportion of DEGs in different cell types at 8 and 36 hpi with *O. heveae*. (e) UpSet plot of DEGs at 8 and 36 hpi with *O. heveae*. The intersection sizes between several cell types in response to *O. heveae* are displayed on the UpSet plot. The height of the bar under each column reflects the number (intersection size) of DEGs ( $|logFC| \geq 0.8, p \leq 0.05$ ) shared by the cell types filled in the matrix. Only the columns with an intersection size not less than 10 are shown. DEG, differentially expressed gene; hpi, hours postinoculation; UMAP, uniform manifold approximation projection; UMI, unique molecular identifier. [Color figure can be viewed at [wileyonlinelibrary.com](http://wileyonlinelibrary.com)]

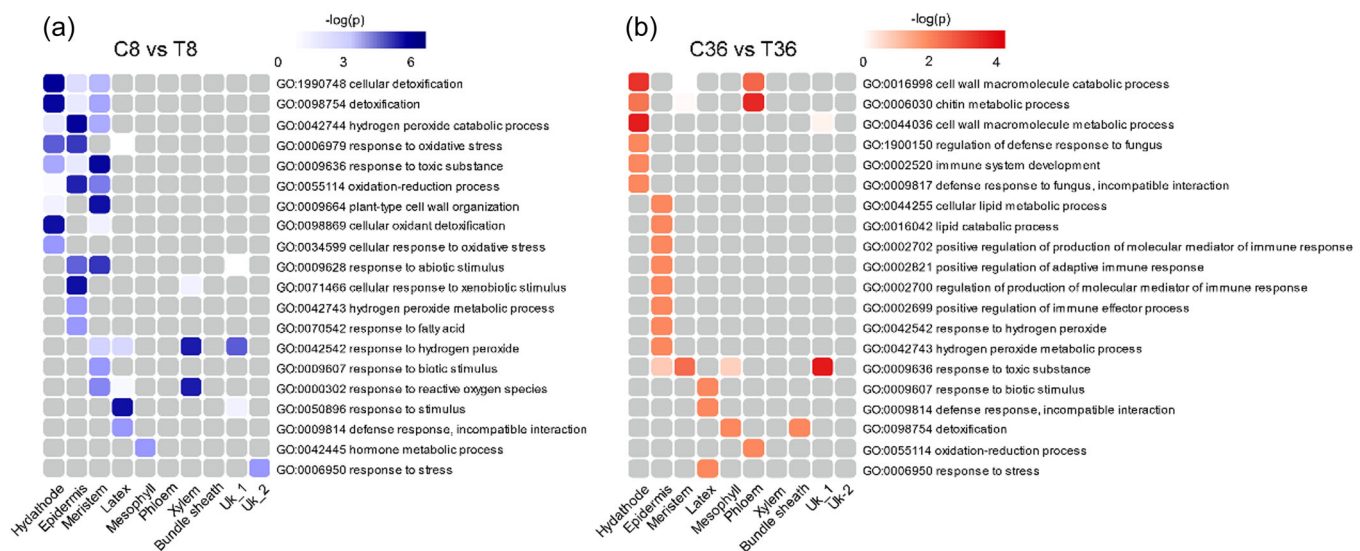


**FIGURE 4** The GO terms of rubber tree leave in response to *Oidium heveae* infection. (a) GO terms enriched in down-regulated DEGs at 8 hpi in multiple cell types ( $p \leq 0.05$ ). (b) GO terms enriched in upregulated DEGs at 36 hpi in multiple cell types ( $p \leq 0.05$ ). DEG, differentially expressed gene; GO, gene ontology; hpi, hours postinoculation. [Color figure can be viewed at [wileyonlinelibrary.com](http://wileyonlinelibrary.com)]

**TABLE 1** KEGG analysis for the genes specifically and differentially expressed of cell clusters in rubber leaves at 8 hpi by *Oidium heveae*.

Cell type	Pathway ID	Description	-log (p)
Hydathode	ko00195	Photosynthesis	5.08
	ko00196	Photosynthesis-antenna proteins	2.79
	ko01200	Carbon metabolism	1.99
	ko00710	Carbon fixation in photosynthetic organisms	1.50
Epidermis	ko00195	Photosynthesis	30.60
	ko00196	Photosynthesis-antenna proteins	25.12
	ko00860	Porphyrin and chlorophyll metabolism	4.09
	ko00710	Carbon fixation in photosynthetic organisms	1.61
	ko01200	Carbon metabolism	1.47
Meristem	ko00195	Photosynthesis	20.31
	ko00196	Photosynthesis-antenna proteins	18.65
Latex	ko00195	Photosynthesis	4.46
	ko00196	Photosynthesis-antenna proteins	5.79
Phloem	ko00195	Photosynthesis	2.13
Bundle sheath	ko00195	Photosynthesis	7.20
	ko01200	Carbon metabolism	2.41
Uk_2	ko00195	Photosynthesis	1.77

Abbreviations: hpi, hours postinoculation; KEGG, Kyoto Encyclopedia of Genes and Genomes.

processing time increased (Figure 5b). Based on the pseudotime value of each epidermal cell, we screened the DEGs along the pseudotime line and performed cluster analysis. The DEGs were grouped into seven clusters by similarity in expression trends (Figure 5c). We analyzed the expression patterns of all genes belonging to the plant-pathogen interaction pathway (KO04626). We found that most interaction-related genes showed a trend of significantly upregulated expression with increasing proposed time (Supporting Information: Table S10). We presume that these upregulated genes play an essential role in plant disease resistance. These roles can be classified into four types according to their functions: NLR-related proteins,

calcium sensors, NADPH oxidases and WRKY transcription factors (Figure 5c). Interestingly, we found that an NLR gene (Hb\_110641499), encoding a typical CNL protein, might play a critical role in the plant host's resistance to powdery mildew.

### 3.7 | Evolutionary relationship and expression pattern of the *HbCNL2* gene

Using the BLAST search function, we obtained 43 sequence-complete candidate genes in the *Hevea* genome, which homologated

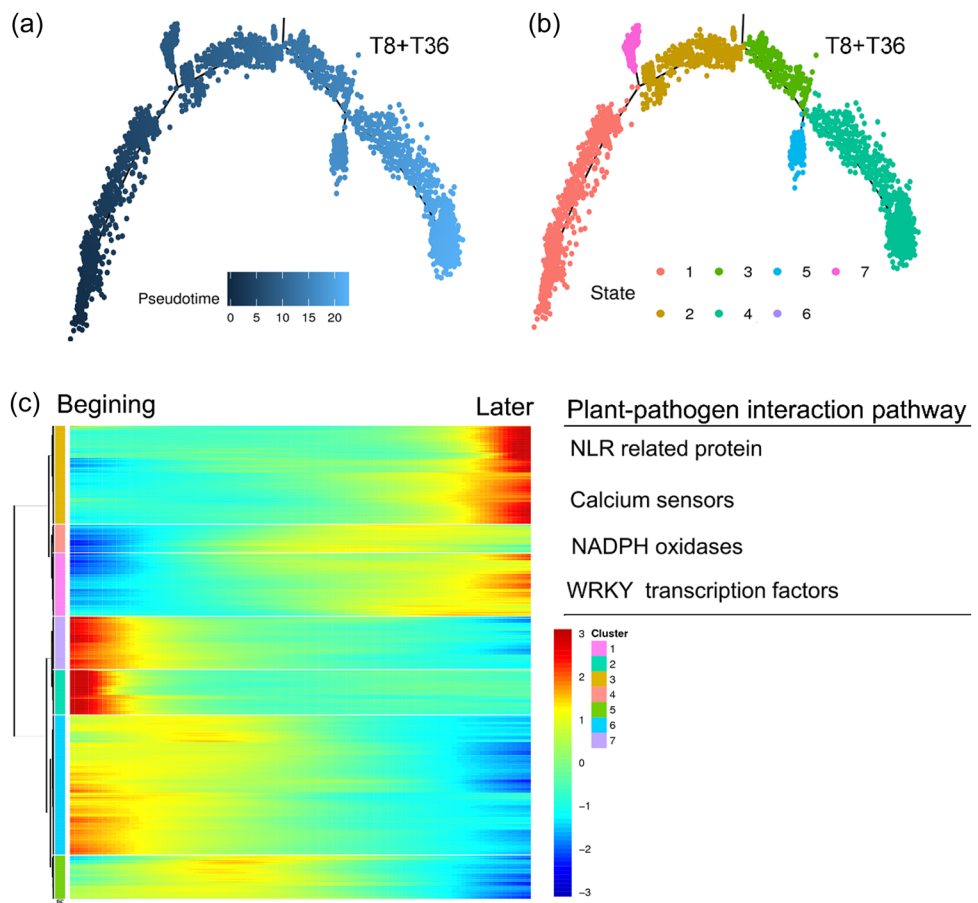


**FIGURE 5** Differentiation trajectory and the fate of epidermal cells of T8 and T36 samples using pseudotime analysis. (a) Pseudotime trajectory. Each dot represents a single cell. (b) Distribution of cells in various states along the cell trajectory. Colours represent different states. (c) Pseudotime heatmap of significantly changed genes. The colour bar indicates the relative gene expression level. NLR, nucleotide-binding leucine-rich. [Color figure can be viewed at [wileyonlinelibrary.com](http://wileyonlinelibrary.com)]

CNL proteins for powdery mildew resistance on barley, wheat and *Dasypyrum* (Supporting Information: Table S11). Phylogenetic trees showed that the six genes encoding typical CNL proteins were noticeably grouped with the CNL proteins of barley and *Dasypyrum* into one cluster (Supporting Information: Figure S6a; Figure 6a). We named these genes *HbCNL1*, *HbCNL2*, *HbCNL3*, *HbCNL4*, *HbCNL5* and *HbCNL6*. Coincidentally, *HbCNL4* is the gene we found in the pseudotime trajectory analysis results. At the overall expression level, these six CNL genes were more highly expressed in moderately resistant (MR) and highly resistant cultivars of rubber trees than in cultivars sensitive to powdery mildew (Figure 6b). Spearman's analysis showed that the expression of the *HbCNL2* gene was significantly correlated ( $p < 0.05$ ) with the level of resistance in these *Hevea* cultivars, with a correlation coefficient of 0.564.

We used the cDNA of *Hevea Renyan* 73397 leaves as a template and successfully cloned the coding sequence of the *HbCNL2* gene, which is 2838 bp in length and encodes 945 amino acids (Supporting Information: Figure S6b). The *HbCNL2* homologous genes (>30% homology) are widely distributed in different plant species and have the same conserved structural domain, implying that these genes play an important biological function in plants (Supporting Information:

Figure S6c). The expression pattern of the *HbCNL2* gene was specific to the rubber tree plant, where the gene expression was significantly higher in leaves than in other tissues (Figure 6c). Expressions of this gene responded conspicuously to the infection of *O. heveae*, surging at 6 h after pathogen inoculation (Figure 6d).

### 3.8 | Subcellular localization and functional analysis of the *HbCNL2* protein

We spliced GFP to the N-terminus of the *HbCNL2* gene and expressed the fusion protein under the control of the constitutive CaMV 35S promoter (35S) in tobacco (*N. benthamiana*) epidermal leaf cells. The overlay of the GFP fluorescence with the dye DAPI staining signal revealed that the GFP-HbCNL2 fusion protein was localized to the cytomembrane but also to the nucleus (Figure 7a). A typical cell death phenotype was observed in the infiltrated area expressing *HbCNL2* (Figure 7b,c). Moreover, we introduced an overexpression plasmid carrying the *HbCNL2* gene into mesophyll protoplasts derived from rubber leaves. Overexpression of the *HbCNL2* gene resulted in higher levels of ROS in protoplasts compared with

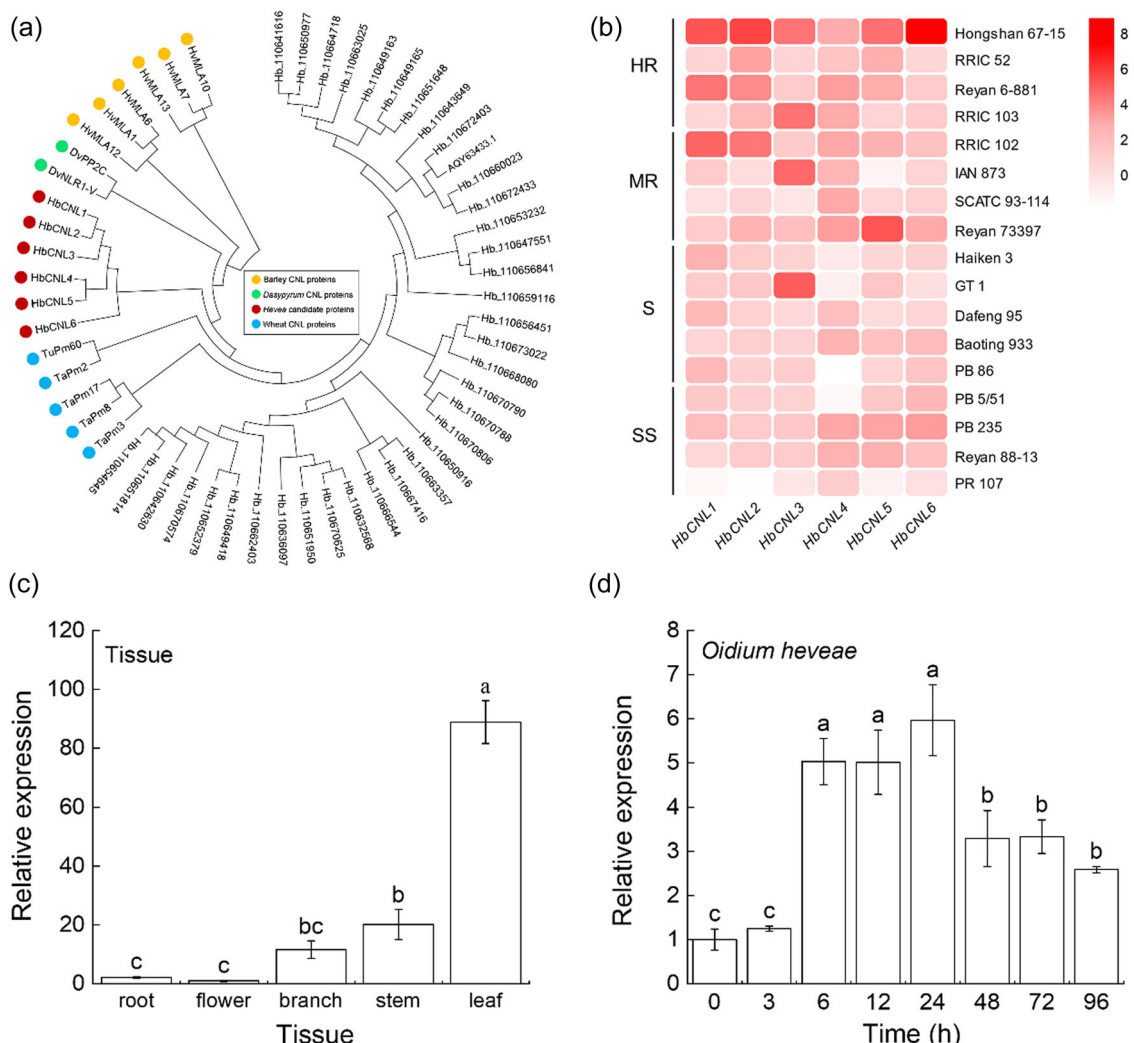


**FIGURE 6** Evolutionary relationship and expression pattern of *HbCNL2* gene. (a) Phylogenetic analyses of *Heveae* proteins with CNL proteins for powdery mildew resistance on barley, wheat and *Dasyperym*. (b) Expression patterns of CNL genes in resistant and sensitive varieties of rubber trees. (c) Expression patterns of the *HbCNL2* gene in different tissues of rubber trees. (d) *HbCNL2* gene expression patterns in response to powdery mildew infection. Columns with different lowercase letters denote significant differences at the  $p < 0.05$  level. HR, highly resistant; MR, moderately resistant; S, sensitive; SS, supersensitive. [Color figure can be viewed at [wileyonlinelibrary.com](http://wileyonlinelibrary.com)]

untransformed protoplasts or protoplasts transformed with an empty plasmid (Figure 5d).

### 3.9 | Protein interaction between HbCNL2 and chaperones

Several chaperone proteins are required for NLR folding and accumulation, including HSP90 and SGT1 (Chapman et al., 2022; Shirasu, 2009). We've successfully identified the *HbHSP90* and *HbSGT1* gene families in rubber trees and revealed the participation of powdery mildew resistance-related genes, *HbHSP90.1* and *HbSGT1b* (Liu et al., 2022; Wang et al., 2023). In this study, we demonstrated the interaction between HbCNL2 and the two chaperones with LCA and BiFC assays (Figure 8a,b; Supporting Information: Figure S7). The results revealed HbCNL2 interacted with

HbHSP90 but not with HbSGT1b. Moreover, the LRR domain of HbCNL2 and the histidine kinase-like ATPase (HATPase) domain of HbHSP90 are consistent with previous reports for the MLA1 and MLA6 proteins in barley (Figure 8c; Bieri et al., 2004).

## 4 | DISCUSSION

Omics techniques have been widely used to screen for disease-resistance genes, but their application has been limited in powdery mildew research. All powdery mildew pathogens are strictly obligate biotrophic pathogens that adhere to the surface of plant tissues. Conventional omics mainly aim to characterize the plant response to pathogens at the whole-tissue level, obscuring the characteristics of different cell populations (Bai et al., 2022). Botany applications of single-cell transcriptomics enable the resolution of plant disease

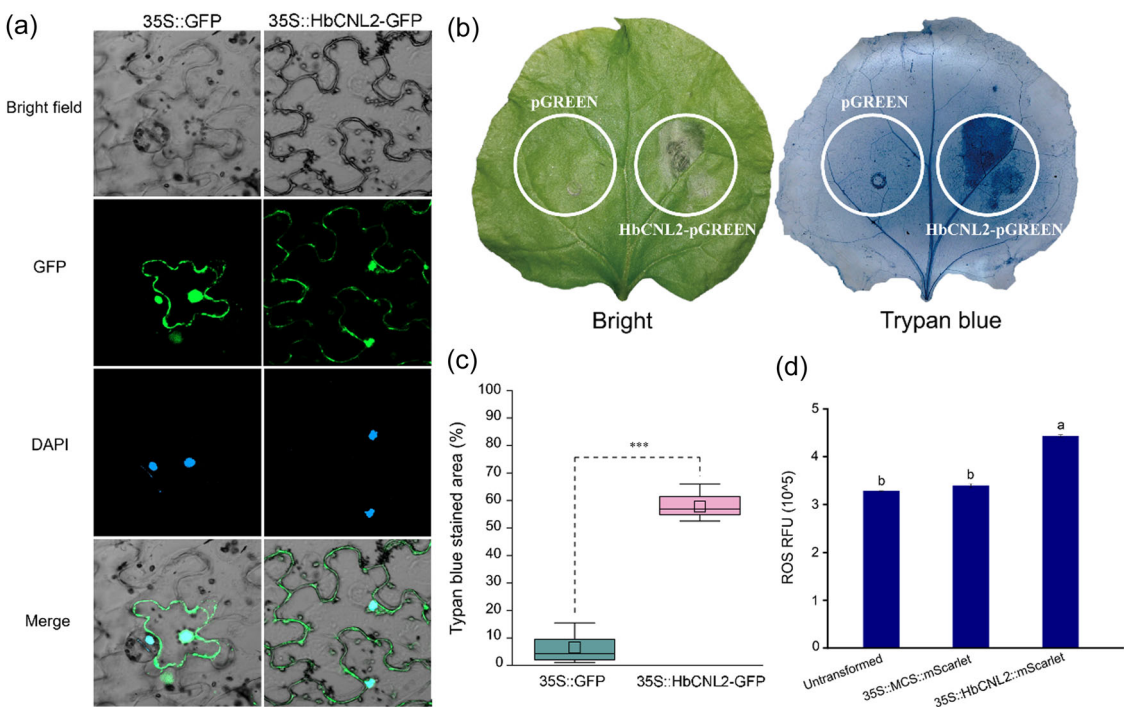


**FIGURE 7** Subcellular localization and functional analysis of HbCNL2 protein. (a) HbCNL2 subcellular localization in tobacco (*Nicotiana benthamiana*) leaves. Bar, 20 µm. (b) Symptoms of trypan blue staining in tobacco expressing HbCNL2. 35::GFP fusion constructs were used as control proteins. (c) Trypan blue staining of a tobacco leaf expressing HbCNL2. \*\*\*p = 0.001. (d) Fluorescence intensities of ROS in protoplasts of rubber leaves overexpressing HbCNL2. 35::MCS::mScarlet fusion constructs were used as control proteins. Columns with different lowercase letters denote significant differences at the p = 0.05 level. GFP, green fluorescent protein; RFU, relative fluorescence unit; ROS, reactive oxygen species. [Color figure can be viewed at [wileyonlinelibrary.com](#)]

resistance processes at the level of individual cell types. For this reason, single-cell sequencing technology may be helpful for researching how obligate biotrophic diseases and plant hosts interact. In this study, we characterized the distinct gene expression patterns of rubber leaf cells during powdery mildew infection and successfully screened a gene for resistance to powdery mildew in rubber trees.

#### 4.1 | Construction of a single-cell atlas of *Hevea* leaves

*Hevea* leaves are compound, digitate leaves with three oblong leaflets. The dorsiventral leaflet blades have an abaxial epidermis, an adaxial epidermis, a uniseriate palisade parenchyma, and a spongy parenchyma with three to four cell layers. Laticifers occur in the phloem region of the veins and between the palisade and spongy parenchyma (Martins and Zieri, 2003). As an early-maturing and high-yielding cultivar, *Hevea* Reyen73397 is currently the most representative cultivar in China's rubber planting areas (Tang et al., 2016). In this study, we successfully isolated high-quality protoplasts from the leaves of Reyen-73397 seedlings by enzyme-induced protoplast generation and captured the major cell types (Figure 1a). Because there are few reports verifying spatiotemporal gene expression patterns in rubber leaves, we tried the same approach that has been used in the single-cell study of tea leaves (Wang et al., 2022). We

annotated the rubber leaf cell type using several known homologous markers from *Arabidopsis*, maize and rice (Figure 1c). Based on the leaf anatomy and conserved gene expression patterns in rubber trees and model plants, we divided rubber leaf cells into 10 cell types. Cells from the mesophyll, epidermis, phloem, xylem, meristem, bundle sheath, hydathode and latex were identified according to the marker genes of different cell clusters (Figure 1d). In addition, we constructed a cluster-specific marker gene library to categorize diverse tissues of rubber trees into specific cell types (Supporting Information: Table S5). The single-cell transcriptome of rubber trees was previously unreported. The single-cell atlas provides a solid basis for further research on the functional characterization and genetic engineering of candidate genes to develop elite cultivars.

#### 4.2 | Cell responses of *Hevea* leaves to powdery mildew infection

In the interactions of powdery mildew with plant leaves, the entry of the penetration peg into an epidermal cell appears to be a key point (Fung et al., 2008). Host cells show distinct gene expression patterns between the prehaustorial and haustorial phases of the powdery mildew (O'Connell & Panstruga, 2006). Previous studies showed that the invasion of *O. heveae* in rubber leaves was mainly divided into four crucial time points: conidia germination peak (4 hpi), appressoria

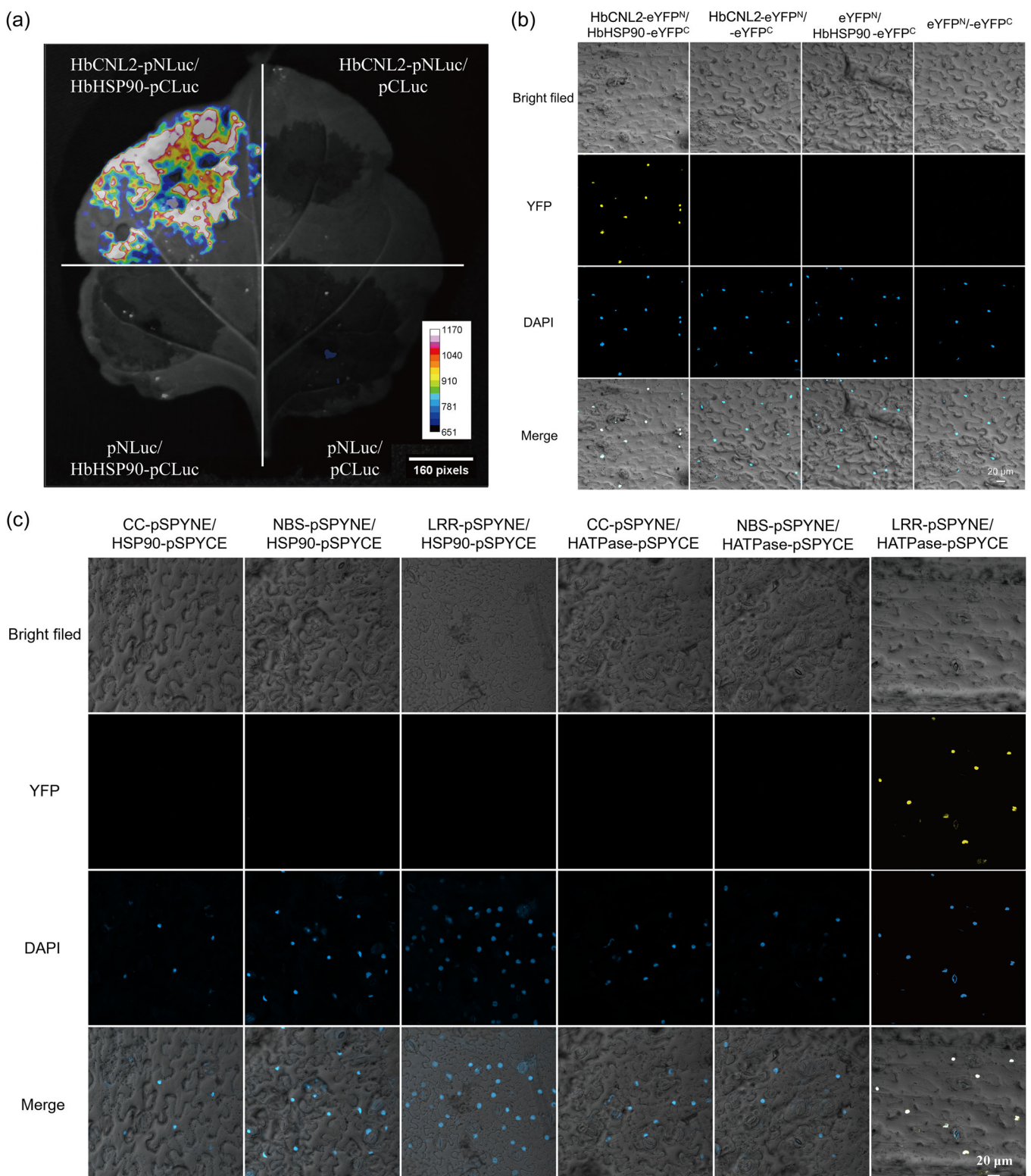


**FIGURE 8** HbCNL2 interacts with HbHSP90 in *Nicotiana benthamiana* leaves. (a) Luciferase complementation imaging of the interaction between HbCNL2 and HbHSP90. Bimolecular fluorescent complexes are created as a result of protein interactions. In contrast, it shows no fluorescence in the absence of protein interactions. (b) Bimolecular fluorescence complementation imaging of the interaction between HbCNL2 and HbHSP90. (c) Domain interaction between HbCNL2 and HbHSP90. The BiFC fluorescence signal is produced when two proteins interact in the cell. Bar, 20 µm. BiFC, bimolecular fluorescence complementation; DAPI, 4',6-diamidino-2-phenylindole; LRR, leucine-rich repeat; NBS, nucleotide-binding site; YFP, yellow fluorescent protein. [Color figure can be viewed at [wileyonlinelibrary.com](http://wileyonlinelibrary.com)]

formation peak (8 hpi), haustoria formation peak (12–15 hpi) and hyphae formation peak (24–36 hpi) (Wan et al., 2014; Zhang et al., 2010). In this study, we chose the time points 8 and 36 hpi for observing the differences in infected-host genes before and after haustorium formation. Meanwhile, we selected healthy leaves at the same inoculation time as controls.

Based on single-cell expression profiles at two key time points during infection, we found that rubber leaf cells were heterogeneous in response to *O. heveae* invasion (Figure 3). Meristem cells appeared to respond strongly to the *O. heveae* stimulus. With a higher cell percentage, epidermal cells exhibited a similar expression pattern to meristem cells. As sessile organisms, plants are exposed to extreme and fluctuating environmental conditions and support stress resilience by increasing cell and genome stability (Rymen & Sugimoto, 2012). All epidermal cells develop from the leaf protoderm created by meristem cells (Zuch et al., 2022). We inferred that rubber leaves resisted *O. heveae* infection by triggering meristem cell activity and increasing the number of epidermal cells. We further identified DEGs at these two infection times and suggested a variable process in the host response to *O. heveae*. At 8 hpi, the majority of 20 enriched immune-related GO terms were significantly down-regulated in hydathode, epidermis and meristem cells (Figure 4a). The reduced expression level of these defence-related genes during the critical period in compatible interactions suggests that *O. heveae* exports fungal factors into host cells that could suppress defence-related genes (Caldo et al., 2004; Panstruga, 2002). Chandran et al. (2010) found diminished photosynthesis and a carbon source to sink transition in *Arabidopsis* cells during powdery mildew infection. Our KEGG analysis also showed that the expression of genes involved in photosynthesis and related processes was significantly decreased in most rubber leaf cells with infection (Table 1). Thus, plant hosts could respond to abiotic stress through an active and adaptive process, such as a decline in photosynthetic efficiency and an increase in cellular ROS (Taleisnik et al., 2009; Teves and Henikoff, 2011). When *O. heveae* had wholly invaded rubber leaves and established a parasitic relationship at 36 hpi, the corresponding host resistance reaction could be generated to prevent further expansion of the pathogen (Ngou et al., 2022; Wan et al., 2014). Most immune-related GO terms were significantly upregulated and enriched mainly in the epidermis and hydathode cells (Figure 4b). Pseudotime trajectory further revealed signals of the transition from normal functioning to defence response in epidermal cells (Figure 5). The state of the epidermal cells changed significantly with pseudotime. The majority of interaction-related genes, primarily those encoding NLR-related proteins, calcium signalling sensors and NADPH oxidases, were significantly upregulated during the middle and late stages of pseudotime. Chandran et al. (2010) also found that genes involved in calcium signalling and redox regulation largely exhibited increased expression at the site of powdery mildew infection in an SA-dependent manner. Therefore, elucidating the regulatory mechanisms that control the expression of these genes among plants is vital for understanding the molecular basis of the host's interaction with powdery mildew.

### 4.3 | The *HbCNL2* gene positively modulates rubber leaf defence to powdery mildew

CNL proteins are critical components of immunity in wheat, barley and *Dasypyrum* and are responsible for defence responses against powdery mildew. We inferred that CNL proteins might play a critical role in the resistance of rubber trees to powdery mildew (Figure 6). Six CNL proteins (*HbCNL1*–*HbCNL6*) of rubber trees were highly homologous to powdery mildew resistance proteins of barley and *Dasypyrum*, where the *HbCNL4* gene was significantly upregulated in the middle and later stages of pseudotime. These CNL genes were more highly expressed in resistant cultivars of rubber trees than in sensitive cultivars. In particular, the expression pattern of *HbCNL2* was significantly correlated with the resistance level of cultivars. This gene was highly expressed in rubber leaves and responded to *O. heveae* infection. Overexpression of the *HbCNL2* gene triggered a typical cell death phenotype of tobacco and higher levels of ROS in protoplasts of rubber leaves. These results indicate that the *HbCNL2* gene positively modulates rubber leaf defence against powdery mildew.

### 4.4 | Subcellular localization and protein interaction of *HbCNL2*

CNL proteins might be localized to multiple subcellular compartments (Caplan et al., 2008). The *MLA10* protein localizes to both the cytoplasm and the nucleus of transiently transformed barley leaf epidermal cells, and the nuclear pool is required for its powdery mildew resistance activity (Cesari et al., 2016). Similarly, the *HbCNL2* protein was localized to both the cytomembrane and nucleus (Figure 7). We inferred that nuclear localization is equally important for its resistance against rubber tree powdery mildew. Powdery mildew resistance CLN proteins generally require the chaperones HSP90 and SGT1 to maintain stable levels. For example, HSP90 interacts with barley *MLA1* and *MLA6* (Bieri et al., 2004; Hubert et al., 2003); SGT1 interacts with barley *MLA1* and acts as a cochaperone of HSP90 and modulates NLR accumulation (Bieri et al., 2004; Leister et al., 2005). Although it did not interact with *HbSGT1b*, the *HbCNL2* protein interacted with *HbHSP90* in the nucleus (Figure 8). We previously found that *HbHSP90* interacts with *HbSGT1b* in the nucleus during stress responses of the rubber tree (Liu et al., 2022). Thus, the HSP90-SGT1 pair might be essential for accumulating and maintaining the stability of NLR protein *HbCNL2* in rubber trees.

## 5 | CONCLUSION

The transcriptional profiles of *Hevea* leaves during early powdery mildew infection were investigated. We first identified 10 cell types using 18 marker genes, constructed a transcriptome atlas, and analyzed the leaf cell responses to powdery mildew infection. The

epidermal cells showed distinct gene expression patterns under powdery mildew infection, and most of the genes involved in host-pathogen interactions were up-expressed along with the infection process. Based on pseudotime trajectories in epidermal cells, we found that a new CNL gene, *HbCNL2*, interacted with *HbHSP90* and positively modulated the defence of *Hevea* leaves against powdery mildew. Thus, the first single-cell transcriptional landscape in rubber tree leaves was reported, and a novel resistance gene to powdery mildew was discovered.

## ACKNOWLEDGEMENTS

This work was supported by grants from the Natural Science Foundation of Innovative Research Team Project of Hainan province (322CXTD506), the National Natural Science Foundation of China (32160370; 32160654) and the Modern Agro-Industry Technology Research System (CARS-33-BC1). We thank the professor Haiyan Li for careful reading of our original manuscript and providing constructive suggestions.

## DATA AVAILABILITY STATEMENT

The data that support the findings of this study are available from the corresponding author upon reasonable request. All sequencing data have been deposited in the Genome Sequence Archive in the National Genomics Data Center, China National Center for Bioinformation, Chinese Academy of Sciences, under the accession number CRA008733. (<https://ngdc.cncb.ac.cn/gsa>).

## ORCID

Xiaoyu Liang  <http://orcid.org/0000-0002-8820-0853>

## REFERENCES

- Bai, Y., Liu, H., Lyu, H., Su, L., Xiong, J. & Cheng, Z.M. (2022) Development of a single-cell atlas for woodland strawberry (*Fragaria vesca*) leaves during early *Botrytis cinerea* infection using single-cell RNA-seq. *Horticulture Research*, 9, uhab055.
- Becht, E., McInnes, L., Healy, J., Dutertre, C.A., Kwok, I.W.H., Ng, L.G. et al. (2019) Dimensionality reduction for visualizing single-cell data using UMAP. *Nature Biotechnology*, 37, 38–44.
- Bieri, S., Mauch, S., Shen, Q.H., Peart, J., Devoto, A., Casais, C. et al. (2004) RAR1 positively controls steady state levels of barley MLA resistance proteins and enables sufficient MLA6 accumulation for effective resistance. *The Plant Cell*, 16, 3480–3495.
- Bourdenx, B., Bernard, A., Domergue, F., Pascal, S., Léger, A., Roby, D. et al. (2011) Overexpression of *Arabidopsis ECERIFERUM1* promotes wax very-long-chain alkane biosynthesis and influences plant response to biotic and abiotic stresses. *Plant Physiology*, 156, 29–45.
- Caldo, R.A., Nettleton, D. & Wise, R.P. (2004) Interaction-dependent gene expression in *Mla*-specified response to barley powdery mildew. *The Plant Cell*, 16, 2514–2528.
- Caplan, J., Padmanabhan, M. & Dinesh-Kumar, S.P. (2008) Plant NB-LRR immune receptors: from recognition to transcriptional reprogramming. *Cell Host & Microbe*, 3, 126–135.
- Cesari, S., Moore, J., Chen, C., Webb, D., Periyannan, S., Mago, R. et al. (2016) Cytosolic activation of cell death and stem rust resistance by cereal MLA-family CC-NLR proteins. *Proceedings of the National Academy of Sciences of the United States of America*, 113, 10204–10209.
- Chandran, D., Inada, N., Hather, G., Kleindt, C.K. & Wildermuth, M.C. (2010) Laser microdissection of *Arabidopsis* cells at the powdery mildew infection site reveals site-specific processes and regulators. *Proceedings of the National Academy of Sciences of the United States of America*, 107, 460–465.
- Chapman, A.V.E., Elmore, J.M., McReynolds, M., Walley, J.W. & Wise, R.P. (2022) SGT1-specific domain mutations impair interactions with the barley MLA6 immune receptor in association with loss of NLR protein. *Molecular Plant-Microbe Interactions*, 35, 274–289.
- Conway, J.R., Lex, A. & Gehlenborg, N. (2017) UpSetR: an R package for the visualization of intersecting sets and their properties. *Bioinformatics*, 33, 2938–2940.
- de Marcos, A., Houbaert, A., Triviño, M., Delgado, D., Martín-Trillo, M., Russinova, E. et al. (2017) A mutation in the bHLH domain of the SPCH transcription factor uncovers a BR-dependent mechanism for stomatal development. *Plant Physiology*, 174, 823–842.
- Dinneny, R., Long, T.A., Wang, J.Y., Jung, J.W., Mace, D., Pointer, S. et al. (2008) Cell identity mediates the response of *Arabidopsis* roots to abiotic stress. *Science*, 320, 942–945.
- Feng, W.Q., Tong, Z., Jin, X., Wang, D., Sun, Y., Meng, X.R. et al. (2016) Cloning and expression of REF/SRPP gene family in rubber tree (*Hevea brasiliensis*). *Molecular Plant Breeding*, 14, 3024–3032.
- Fung, R.W.M., Gonzalo, M., Fekete, C., Kovacs, L.G., He, Y., Marsh, E. et al. (2008) Powdery mildew induces defense-oriented reprogramming of the transcriptome in a susceptible but not in a resistant grapevine. *Plant Physiology*, 146, 236–249.
- Girard, A.L., Mounet, F., Lemaire-Chamley, M., Gaillard, C., Elmorjani, K., Vivancos, J. et al. (2012) Tomato GDSL1 is required for cutin deposition in the fruit cuticle. *The Plant Cell*, 24, 3119–3134.
- Gottwald, J.R., Krysan, P.J., Young, J.C., Evert, R.F. & Sussman, M.R. (2000) Genetic evidence for the in planta role of phloem-specific plasma membrane sucrose transporters. *Proceedings of the National Academy of Sciences of the United States of America*, 97, 13979–13984.
- Hu, Y., Li, Y., Hou, F., Wan, D., Cheng, Y., Han, Y. et al. (2018) Ectopic expression of *Arabidopsis* broad-spectrum resistance gene RPW8.2 improves the resistance to powdery mildew in grapevine (*Vitis vinifera*). *Plant Science*, 267, 20–31.
- Hubert, D.A., Tornero, P., Belkhadir, Y., Krishna, P., Takahashi, A., Shirasu, K. et al. (2003) Cytosolic HSP90 associates with and modulates the *Arabidopsis RPM1* disease resistance protein. *The EMBO Journal*, 22, 5679–5689.
- Jean-Baptiste, K., McFadie-Figueroa, J.L., Alexandre, C.M., Dorrrity, M.W., Saunders, L., Bubb, K.L. et al. (2019) Dynamics of gene expression in single root cells of *Arabidopsis thaliana*. *The Plant Cell*, 31, 993–1011.
- Keogh, R.C., Deverall, B.J. & McLeod, S. (1980) Comparison of histological and physiological responses to *Phakopsora pachyrhizi* in resistant and susceptible soybean. *Transactions of the British Mycological Society*, 74, 329–333.
- Kim, J.-Y., Symeonidi, E., Pang, T.Y., Denyer, T., Weidauer, D., Bezrutczyk, M. et al. (2021) Distinct identities of leaf phloem cells revealed by single cell transcriptomics. *The Plant Cell*, 33, 511–530.
- Lambertucci, S., Orman, K.M., Das Gupta, S., Fisher, J.P., Gazal, S., Williamson, R.J. et al. (2019) Analysis of barley leaf epidermis and extrahaustorial proteomes during powdery mildew infection reveals that the PR5 thaumatin-like protein TLP5 is required for susceptibility towards *Blumeria graminis* f. sp. *hordei*. *Frontiers in Plant Science*, 10, 1138.
- Leister, R.T., Dahlbeck, D., Day, B., Li, Y., Chesnokova, O. & Staskawicz, B.J. (2005) Molecular genetic evidence for the role of SGT1 in the intramolecular complementation of Bs2 protein activity in *Nicotiana benthamiana*. *The Plant Cell*, 17, 1268–1278.
- Li, H., Dai, X., Huang, X., Xu, M., Wang, Q., Yan, X. et al. (2021) Single-cell RNA sequencing reveals a high-resolution cell atlas of xylem in *Populus*. *Journal of Integrative Plant Biology*, 63, 1906–1921.

- Li, M., Dong, L., Li, B., Wang, Z., Xie, J., Qiu, D. et al. (2020) A CNL protein in wild emmer wheat confers powdery mildew resistance. *New Phytologist*, 228, 1027–1037.
- Liang, P., Liu, S., Xu, F., Jiang, S., Yan, J., He, Q. et al. (2018) Powdery mildews are characterized by contracted carbohydrate metabolism and diverse effectors to adapt to obligate biotrophic lifestyle. *Frontiers in Microbiology*, 9, 3160.
- Liu, H., Hu, D., Du, P., Wang, L., Liang, X., Li, H. et al. (2021) Single-cell RNA-seq describes the transcriptome landscape and identifies critical transcription factors in the leaf blade of the allotetraploid peanut (*Arachis hypogaea* L.). *Plant Biotechnology Journal*, 19, 2261–2276.
- Liu, M., Wang, L., Ke, Y., Xian, X., Wang, J., Wang, M. et al. (2022) Identification of *HbHSP90* gene family and characterization *HbHSP90*. 1 as a candidate gene for stress response in rubber tree. *Gene*, 827, 146475.
- Liu, Z., Zhou, Y., Guo, J., Li, J., Tian, Z., Zhu, Z. et al. (2020) Global dynamic molecular profiling of stomatal lineage cell development by single-cell RNA sequencing. *Molecular Plant*, 13, 1178–1193.
- Liyanage, K.K., Khan, S., Mortimer, P.E., Hyde, K.D., Xu, J., Brooks, S. et al. (2016) Powdery mildew disease of rubber tree. *Forest Pathology*, 46, 90–103.
- Lu, S., Yi, S.S., Li, C.H., Liao, Y. & Yin, J.M. (2018) Research progress of promoters on horticultural plants. *Northern Horticulture*, 16, 185–195.
- Maaten, L.v.d. & Hinton, G. (2008) Visualizing data using t-SNE. *Journal of Machine Learning Research*, 9, 2579–2605.
- Martins, M.B.G. & Zieri, R. (2003) Leaf anatomy of rubber-tree clones. *Scientia Agricola*, 60, 709–713.
- Narayanan, C. & Mydin, K.K. (2012) Breeding for disease resistance in *Hevea* spp.—status, potential threats and possible strategies. In: *Proceedings of the 4th International Workshop on Genetics of Host-Parasite Interactions in Forestry*. pp. 240–251.
- Ngou, B.P.M., Ding, P. & Jones, J.D.G. (2022) Thirty years of resistance: zig-zag through the plant immune system. *The Plant Cell*, 34, 1447–1478.
- O'Connell, R.J. & Panstruga, R. (2006) Tête à tête inside a plant cell: establishing compatibility between plants and biotrophic fungi and oomycetes. *New Phytologist*, 171, 699–718.
- Palit, P., Ghosh, R., Tolani, P., Tarafdar, A., Chitikineni, A., Bajaj, P. et al. (2020) Molecular and physiological alterations in chickpea under elevated CO<sub>2</sub> concentrations. *Plant and Cell Physiology*, 61, 1449–1463.
- Panstruga, R. & Schulze-Lefert, P. (2002) Live and let live: insights into powdery mildew disease and resistance. *Molecular Plant Pathology*, 3, 495–502.
- Priyadarshan, P.M. & Goncalves, P.S. (2003) *Hevea* gene pool for breeding. *Genetic Resources and Crop Evolution*, 50, 101–114.
- Reina, J.J., Guerrero, C. & Heredia, A. (2007) Isolation, characterization, and localization of *AgaSGNH* cDNA: a new SGNH-motif plant hydrolase specific to *Agave americana* L. leaf epidermis. *Journal of Experimental Botany*, 58, 2717–2731.
- Rich-Griffin, C., Stechemesser, A., Finch, J., Lucas, E., Ott, S. & Schäfer, P. (2020) Single-cell transcriptomics: a high-resolution avenue for plant functional genomics. *Trends in Plant Science*, 25, 186–197.
- Rymen, B. & Sugimoto, K. (2012) Tuning growth to the environmental demands. *Current Opinion in Plant Biology*, 15, 683–690.
- Satterlee, J.W., Strable, J. & Scanlon, M.J. (2020) Plant stem-cell organization and differentiation at single-cell resolution. *Proceedings of the National Academy of Sciences of the United States of America*, 117, 33689–33699.
- Seeholzer, S., Tsuchimatsu, T., Jordan, T., Bieri, S., Pajonk, S., Yang, W. et al. (2010) Diversity at the *Mla* powdery mildew resistance locus from cultivated barley reveals sites of positive selection. *Molecular Plant-Microbe Interactions*, 23, 497–509.
- Shirasu, K. (2009) The HSP90-SGT1 chaperone complex for NLR immune sensors. *Annual review of plant biology*, 60, 139–164.
- Stoppel, R., Lezhneva, L., Schwenkert, S., Torabi, S., Felder, S., Meierhoff, K. et al. (2011) Recruitment of a ribosomal release factor for light- and stress-dependent regulation of petB transcript stability in *Arabidopsis* chloroplasts. *The Plant Cell*, 23, 2680–2695.
- Taleisnik, E., Rodríguez, A.A., Bustos, D., Erdei, L., Ortega, L. & Senn, M.E. (2009) Leaf expansion in grasses under salt stress. *Journal of Plant Physiology*, 166, 1123–1140.
- Tang, C., Yang, M., Fang, Y., Luo, Y., Gao, S., Xiao, X. et al. (2016) The rubber tree genome reveals new insights into rubber production and species adaptation. *Nature Plants*, 2, 16073.
- Teves, S.S. & Henikoff, S. (2011) Heat shock reduces stalled RNA polymerase II and nucleosome turnover genome-wide. *Genes & Development*, 25, 2387–2397.
- Tsutsumi, K., Taniguchi, Y., Kawasaki, M., Taniguchi, M. & Miyake, H. (2006) Expression of photosynthesis-related genes during the leaf development of a C<sub>3</sub> plant rice as visualized by *in situ* hybridization. *Plant Production Science*, 9, 232–241.
- van Raemdonck, D., Pesquet, E., Cloquet, S., Beeckman, H., Boerjan, W., Goffner, D. et al. (2005) Molecular changes associated with the setting up of secondary growth in aspen. *Journal of Experimental Botany*, 56, 2211–2227.
- van Wersch, S., Tian, L., Hoy, R. & Li, X. (2020) Plant NLRs: the whistleblowers of plant immunity. *Plant Communications*, 1, 100016.
- Wan, S.L., Liang, P., Liu, W.B., Zhang, Y., Miao, W.G. & Zheng, F.C. (2014) Cytological analysis of compatible interactions between rubber tree and *Oidium heveae*. *Plant Production*, 40, 36.
- Wang, Y., Huan, Q., Li, K. & Qian, W. (2021) Single-cell transcriptome atlas of the leaf and root of rice seedlings. *Journal of Genetics and Genomics*, 48, 881–898.
- Wang, Q., Wu, Y., Peng, A., Cui, J., Zhao, M.Y., Pan, Y.T. et al. (2022) Single-cell transcriptome atlas reveals developmental trajectories and a novel metabolic pathway of catechin esters in tea leaves. *Plant Biotechnology Journal*, 20, 2089–2106.
- Wang, M., Xiao, H.X., Li, X.M., Wan, S.L., Yang, Y., Yu, H.Y. et al. (2023) Functional characterization of powdery mildew resistance-related genes *HbSGT1a* and *HbSGT1b* in *Hevea brasiliensis* Muell. Arg. *European Journal of Plant Pathology*, 165, 153–161.
- Xiao, S., Ellwood, S., Calis, O., Patrick, E., Li, T., Coleman, M. et al. (2001) Broad-spectrum mildew resistance in *Arabidopsis thaliana* mediated by *RPW8*. *Science*, 291, 118–120.
- Xu, X., Crow, M., Rice, B.R., Li, F., Harris, B., Liu, L. et al. (2021) Single-cell RNA sequencing of developing maize ears facilitates functional analysis and trait candidate gene discovery. *Developmental Cell*, 56, 557–568.
- Yeats, T.H., Howe, K.J., Matas, A.J., Buda, G.J., Thannhauser, T.W. & Rose, J.K.C. (2010) Mining the surface proteome of tomato (*Solanum lycopersicum*) fruit for proteins associated with cuticle biogenesis. *Journal of Experimental Botany*, 61, 3759–3771.
- Yu, G., Wang, L.G., Han, Y. & He, Q.Y. (2012) ClusterProfiler: an R package for comparing biological themes among gene clusters. *Omics: A Journal of Integrative Biology*, 16, 284–287.
- Zhang, X., Liu, X. & Wang, J. (2010) Ultrastructural studies on the interaction of rubber tree with *Oidium heveae*. *Chinese Journal of Tropical Crops*, 31, 2250–2254.
- Zhang, X., Wang, L., He, C. & Luo, H. (2016) An efficient transient mesophyll protoplast system for investigation of the innate immunity responses in the rubber tree (*Hevea brasiliensis*). *Plant Cell, Tissue and Organ Culture*, 126, 281–290.
- Zhao, Y., Liu, Q. & Davis, R.E. (2004) Transgene expression in strawberries driven by a heterologous phloem-specific promoter. *Plant Cell Reports*, 23, 224–230.

Zuch, D.T., Doyle, S.M., Majda, M., Smith, R.S., Robert, S. & Torii, K.U. (2022) Cell biology of the leaf epidermis: fate specification, morphogenesis, and coordination. *The Plant Cell*, 34, 209–227.

#### SUPPORTING INFORMATION

Additional supporting information can be found online in the Supporting Information section at the end of this article.

**How to cite this article:** Liang, X., Ma, Z., Ke, Y., Wang, J., Wang, L., Qin, B. et al. (2023) Single-cell transcriptomic analyses reveal cellular and molecular patterns of rubber tree response to early powdery mildew infection. *Plant, Cell & Environment*, 46, 2222–2237.

<https://doi.org/10.1111/pce.14585>